PHYSICAL REVIEW B **85**, 100504(R) (2012)

Optical conductivity of superconducting $Rb_2Fe_4Se_5$ single crystals

A. Charnukha,[1] J. Deisenhofer,[2] D. Pröpper,[1] M. Schmidt,[2] Z. Wang,[2] Y. Goncharov,[2,3] A. N. Yaresko,[1] V. Tsurkan,[2,4] B. Keimer,[1] A. Loidl,[2] and A. V. Boris[1]

[1]*Max-Planck-Institut für Festkörperforschung, Heisenbergstrasse 1, D-70569 Stuttgart, Germany*

[2]*Experimental Physics V, Center for Electronic Correlations and Magnetism, Institute of Physics, University of Augsburg, D-86159 Augsburg, Germany*

[3]*Institute of General Physics, Russian Academy of Sciences, 119991 Moscow, Russia*

[4]*Institute of Applied Physics, Academy of Sciences of Moldova, MD-2028 Chisinau, R. Moldova*

(Received 26 August 2011; revised manuscript received 11 November 2011; published 6 March 2012)

We report the complex dielectric function of high-quality nearly-stoichiometric $Rb_2Fe_4Se_5$ single crystals with $T_c = 32$ K determined by wide-band spectroscopic ellipsometry and time-domain transmission spectroscopy in the spectral range of 1 meV $\leqslant \hbar\omega \leqslant$ 6.5 eV at temperatures of 4 K $\leqslant T \leqslant$ 300 K. This compound simultaneously displays a superconducting and a semiconducting optical response. It reveals a direct band gap of $\approx$0.45 eV determined by a set of spin-controlled interband transitions. Below 100 K, in the lowest terahertz spectral range, we observe a clear metallic response characterized by the negative dielectric permittivity ε_1 and bare (unscreened) $\omega_{pl} \approx 100$ meV. At the superconducting transition, this metallic response exhibits a signature of a superconducting gap below 8 meV. Our findings suggest a coexistence of superconductivity and magnetism in this compound as two separate phases.

DOI: 10.1103/PhysRevB.85.100504 PACS number(s): 74.70.Xa, 74.25.Gz, 71.15.Mb

In the family of iron-pnictide/chalcogenide superconductors, so far, most research efforts have been applied to the so-called 122 compounds with Fe-As conducting planes due to the high quality and large size of the single crystals available. They bear all the hallmarks of this class of superconductors, such as an itinerant antiferromagnetic ground state of the parent compounds, multiple bands crossing the Fermi level, superconducting transition temperatures up to 40 K, and a resonance peak in the inelastic neutron-scattering signal at a (0,0.5,0) or (0.5,0,0) **Q**-vector in the superconducting state,[1] suggesting novel superconductivity with *s*-wave symmetry and a sign change in the order parameter between the hole and the electron Fermi pockets.[2] Throughout the phase diagram, these compounds are metals with a plasma frequency of $\omega_{pl} \approx 1.6$ eV.[3–5] In the superconducting state, the corresponding optical conductivity is fully suppressed below 2Δ due to the formation of a superconducting condensate with a London penetration depth of $\lambda_L \approx 220$ nm.[6–8]

Recently, iron-selenide compounds have been synthesized in this class of superconductors.[9–12] Initially, they were believed to crystallize in the same $I4/mmm$ symmetry of the $ThCr_2Si_2$ type as their iron-arsenide counterparts, but soon it became clear that there is an inherent iron-deficiency order present in these materials with a chiral $\sqrt{5} \times \sqrt{5} \times 1$ superstructure, which reduces the symmetry to $I4/m$ and makes it more appropriate to classify these materials into the 245 stoichiometry.[13] The Fe-defect and antiferromagnetic orders occur at rather high-transition temperatures of 400–550 K. Neutron-scattering studies showed that these compounds possess a magnetic moment on iron atoms of about 3.3 μ_B,[14] which is unusually large for iron pnictides. At the same time, a resonance peak has been observed by the inelastic neutron scattering below $T_c \approx 32$ K at an energy of $\hbar\omega_{res} = 14$ meV and the **Q**-vector (0.5,0.25,0.5) in the unfolded Fe-sublattice notation,[15] which is also unprecedented for the iron pnictides. It is still under debate how superconductivity with such a high transition temperature can exist on such a strong magnetic background, although there are some indications of an inherent phase separation in iron chalcogenides.[16–18] A further complication arises from the fact that, unlike their 122 counterparts, 245 iron selenides show a semiconducting optical response, and, so far, no free-charge-carrier conductivity has been reported.[19]

In this Rapid Communication, we provide evidence for a free-charge-carrier contribution to the optical response in $Rb_2Fe_4Se_5$ (RFS). We show that the charge-carrier density is small with $\omega_{pl} \approx 100$ meV. This metallic response experiences a weak modification upon cooling into the superconducting state. This evidence together with the results of resistivity, magnetization, specific-heat measurements,[20] and Mössbauer spectroscopy[21] indicate that, in this compound, superconductivity and magnetism coexist as two separate phases.

The optimally-doped superconducting RFS single crystals were grown by the Bridgman method (batch BR16 in Ref. 20). From dc resistivity, magnetization, and specific-heat measurements,[20] we obtained $T_c \approx 32$ K. Sample cleaving and handling were carried out in an argon atmosphere at all times prior to every optical measurement. The complex dielectric function $\varepsilon(\omega) = \varepsilon_1(\omega) + i\varepsilon_2(\omega) = 1 + 4\pi i\sigma(\omega)/\omega$, where $\sigma(\omega)$ is the complex optical conductivity, was obtained in the range of 0.01–6.5 eV using broadband ellipsometry as described in Ref. 22. Time-domain terahertz (THz) transmission measurements were carried out in the 1–10-meV spectral range using a TPS spectra 3000 spectrometer with $f/2$ focusing optics (TeraView Ltd.). The transmitted intensity and phase, obtained via a Fourier transform of the time-domain spectra, were used to directly calculate the complex dielectric function. The far-infrared optical response was measured at the infrared beamline of the ANKA synchrotron light source at Karlsruhe Institute of Technology, Germany.

The imaginary and real parts of the complex dielectric function in the 0.01–6.5-eV spectral range are shown in Figs. 1(a) and 1(b), respectively. Down to 10 meV, the

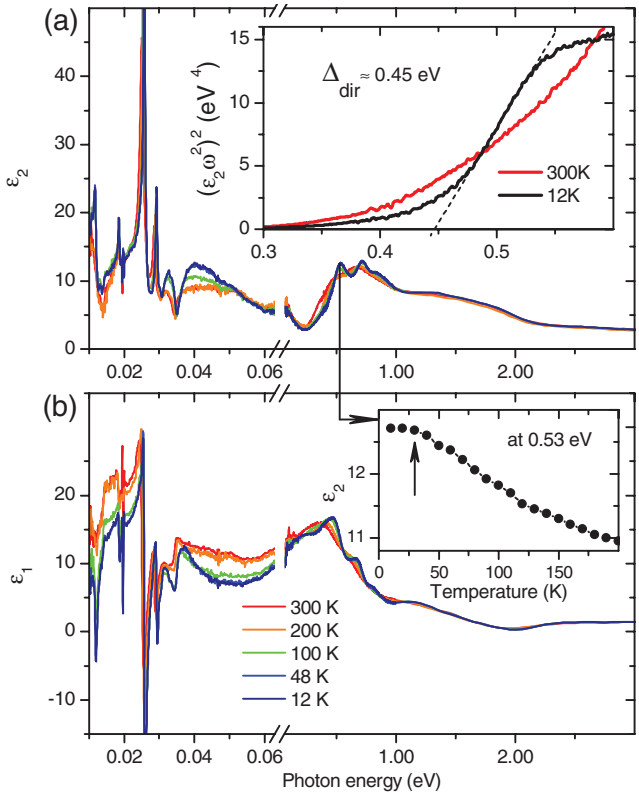

FIG. 1. (Color online) (a) Imaginary and (b) real parts of the dielectric function of RFS in the 0.01–6.5 eV spectral range at different temperatures. [Inset in (a)] Plot of $[\varepsilon_2(\omega)\omega^2]^2$ near the absorption edge. The intersection of the dashed line with the energy axis defines the direct energy gap $\Delta_{dir} = 0.45$ eV at 12 K. [Inset in (b)] Temperature dependence of $\epsilon_2(0.53$ eV).

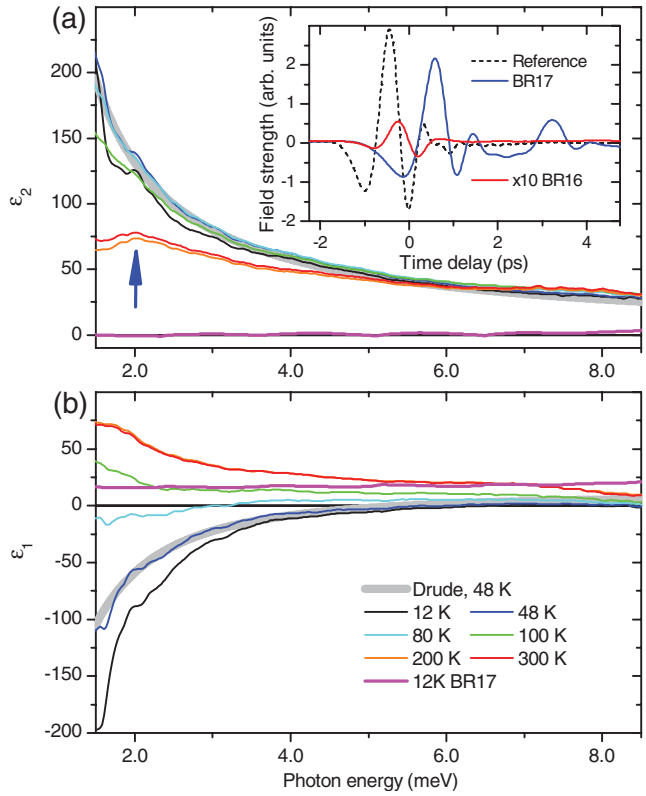

FIG. 2. (Color) (a) Imaginary and (b) real parts of the dielectric function of RFS in the THz spectral region obtained via the time-domain transmission spectroscopy. The blue arrow marks a low-energy electronic excitation. Thick gray lines show a Drude fit to $\varepsilon_1(\omega)$ and $\varepsilon_2(\omega)$ as described in the text. (Inset) Electric-field transients transmitted through a 25-μm-thick superconducting sample (scaled by 10, red line) and a 100-μm-thick transparent insulating sample (blue line). The dashed line plots the reference signal.

sample does not reveal any metallic behavior as is evident from ε_1, which remains positive at all temperatures. It also displays several infrared-active optical phonons, similar to those previously observed in the far-infrared optical response of a semiconducting $K_2Fe_4Se_5$ (KFS).[19] More infrared-active phonons observed than allowed by tetragonal symmetry of the 122 unit cell support the reduction of the Brillouin zone due to the ordering of iron vacancies. Throughout the far-infrared 10–100-meV spectral range, we find a rapid increase of the electronic background in $\sigma_1(\omega)$ between 200 and 100 K with a concomitant decrease in ε_1. At higher frequencies, the optical response features the onset of interband transitions around 0.25 eV. It is followed by an absorption edge at $\approx$0.45 eV formed by direct interband transitions as shown in the inset of Fig. 1(a). Unlike in 122 compounds,[3] the lowest-lying absorption band peaked at about 0.6 eV reveals three separate contributions at low temperatures similar to the two contributions reported for the semiconducting KFS.[19] The inset in Fig. 1(b) shows the strong temperature dependence of one of these absorption bands in the magnetic state, which is linear in a broad temperature range. This behavior is fully consistent with the temperature dependence of the magnetic Bragg peak intensity, including the saturation at 30–40 K,[23] which suggests the spin-controlled character of these interband transitions.

As the compound remains transparent down to 10 meV, a pathway opens to apply time-domain transmission spectroscopy to obtain the complex dielectric function of RFS also at THz frequencies should sufficiently thin samples be obtained. It was indeed possible to achieve sizable transmission in cleaved flakes of RFS about 25-μm thick with terraces less than 100-nm high over 50 $\times$ 50-μm^2 areas. Figures 2(a) and 2(b) show $\varepsilon_2(\omega)$ and $\varepsilon_1(\omega)$, respectively, obtained in the 1–10-meV spectral range using this technique for temperatures of $4 \leqslant T \leqslant 300$ K, along with the optical response of a 100-μm-thick insulating sample BR17 grown by the same method.[20] In the time-domain signal of the insulating sample, the first reflection is clearly visible about 3 ps after the main pulse and results in a superposed interference pattern on its complex dielectric constant. This sample shows a typical frequency-independent insulating response even at 12 K (magenta lines in Fig. 2). Typical electric-field transients obtained on these samples are shown in the inset. The superconducting sample shows much stronger absorption (solid red line) than the insulating one (solid blue line) due to the high level of the electronic background in $\varepsilon_2(\omega)$. At room temperature and down to 100 K, the former remains semiconducting, with $\varepsilon_1(\omega)$ positive in the whole spectral range. However, unlike the insulating sample [thick magenta line in Fig. 2(b)], it exhibits an upturn

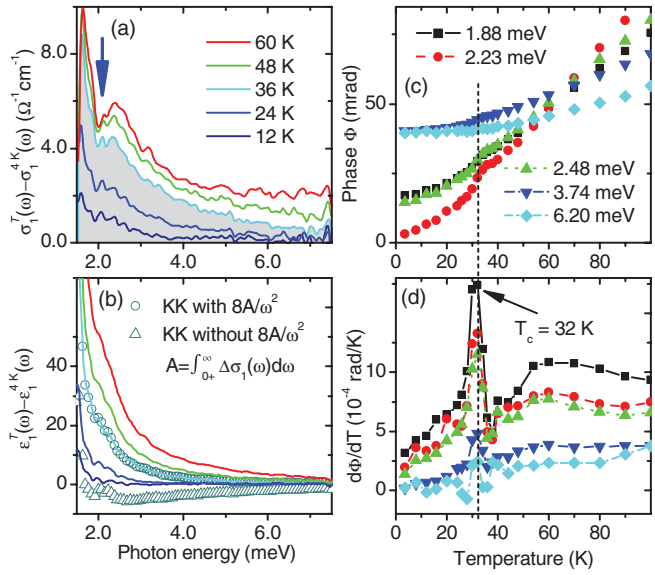

FIG. 3. (Color) Difference spectra (a) $\sigma_1(T,\omega) - \sigma_1(4\text{ K},\omega)$ and (b) $\varepsilon_1(T,\omega) - \varepsilon_1(4\text{ K},\omega)$ of a 25-μm superconducting sample. The blue arrow marks the same low-energy electronic excitation as in Fig. 2(a). Kramers-Kronig transformation of the difference spectrum $\Delta\sigma_1^{36-12\text{ K}}(\omega)$ [cyan line in (a)] with (circles) and without (triangles) the superconductivity-induced term $8A/\omega^2$. The shaded area indicates the spectral weight used to estimate the ω_{pl} of the superconducting condensate (see text). (c) Temperature dependence of the time-domain transmission phase and (d) its temperature derivative for several frequencies. Superconducting transition temperature of 32 K (dashed line).

in $\varepsilon_1(\omega)$ at lowest energies, which indicates a low-energy electronic mode peaked at 2 meV [blue arrow in Fig. 2(a)]. Below 100 K, a clear metallic response with negative $\varepsilon_1(\omega)$ rapidly develops. Already at 80 K, the zero-crossing in $\varepsilon_1(\omega)$ corresponds to a screened plasma frequency of 3 meV, which reaches 6.5 meV as the temperature is lowered further. The metallic response can be fitted by two Drude terms with $\omega_{\text{pl},1} \approx 20$, $\gamma_1 \approx 1$ and $\omega_{\text{pl},2} \approx 95$, $\gamma_2 \approx 40$ meV for the plasma frequencies and scattering rates of the narrow and broad components at 48 K, respectively (thick gray lines in Fig. 2). The total charge-carrier density is given by $\omega_{\text{pl}} = \sqrt{\omega_{\text{pl},1}^2 + \omega_{\text{pl},2}^2} \approx 100$ meV. The observed crossover from semiconducting to metallic behavior with decreasing temperatures below 100 K is in full agreement with the temperature dependence of the dc resistivity.[20] The spectral weight of the low-energy electronic mode in the semiconducting state amounts to about 4% of the total spectral weight of the free charge carriers and might originate from the narrow Drude component. This low-energy mode can represent a collective electronic excitation pinned by structural defects, such as iron vacancies.

The discovery of itinerant charge carriers in the optimally-doped RFS requires a more detailed study of its low-temperature optical response in the vicinity of the superconducting transition temperature. Difference spectra of the real parts of the optical conductivity and the dielectric function are shown in Figs. 3(a) and 3(b), respectively, for several temperatures between 12 and 60 K. The sample shows moderate changes in the normal state and a rapid decrease in the optical conductivity below T_c. The independently-obtained in our experiments $\Delta\varepsilon_1(\omega)$ and $\Delta\sigma_1(\omega) = \Delta\varepsilon_2(\omega)\omega/4\pi$ between the normal (36 K) and superconducting (4 K) state must satisfy the Kramers-Kronig relation:[4] $\Delta\varepsilon_1(\omega) = 8A/\omega^2 + 8\wp\int_{0+}^{\infty}\Delta\sigma_1(x)/(x^2-\omega^2)dx$, where $A = (\omega_{\text{pl}}^{\text{SC}})^2/8$ is the missing area shown in gray in Fig. 3(a). The presence of the first term provides an unambiguous proof for the formation of the superconducting condensate. Figure 3(b) shows that this term is clearly required to reach an adequate agreement between the Kramers-Kronig transformation of the difference spectrum $\Delta\sigma_1^{36-12\text{ K}}(\omega)$ (open symbols) and the independently obtained $\Delta\varepsilon_1^{36-12\text{ K}}(\omega)$ (cyan line). Using this analysis, we determine the superconducting plasma frequency $\omega_{\text{pl}}^{\text{SC}} \approx (40 \pm 16)$ meV, where the uncertainty is due to different possible extrapolations of $\Delta\sigma_1(\omega)$ to zero frequency. Further evidence for the superconductivity-induced nature of these changes in the optical response comes from the temperature dependence of the transmission phase shown in Fig. 3(c) for several frequencies. At all frequencies up to 8 meV, there is a kink at $T_c \approx 32$ K, which gets progressively smaller as the frequency increases. This effect is more obvious in the temperature derivative of the transmission phase shown for the same frequencies in Fig. 3(d). In addition, we observe a double-peak structure around 2 meV [blue arrow in Fig. 3(a); see also Fig. 2(a)], which is overwhelmed by the electronic background at 300 K but clearly stands out at lower temperatures due to reduced electron scattering and even persists in the superconducting state. This feature might have its origin in the electron and hole bound states induced by iron vacancies recently observed at similar energies in a scanning-tunneling-microscopy/spectroscopy study on KFS in Ref. 17, which might serve as pinning centers for a collective electronic excitation.

The striking similarity of the temperature dependence of the triplet feature shown in the inset of Fig. 1(b) to that of the magnetic Bragg peak intensity,[23] both of which exhibit an anomaly at the superconducting transition temperature, might indicate an intimate connection between superconductivity and magnetism in iron chalcogenides. It has also been suggested that the origin of such doublet/triplet features in the optical conductivity of iron selenides is very different from the virtually isostructural 122 iron arsenides.[19] Therefore, it becomes important to determine the nature of these interband transitions. It is known that local-density approximation (LDA) calculations provide an adequate description of the band structure and optical conductivity of iron pnictides[4,24,25] as long as a moderate mass and bandwidth renormalization is taken into account. We compare the experimentally obtained $\sigma_1(\omega)$ with the theoretical prediction for the RFS compound. The calculation was performed for the experimental $\sqrt{5} \times \sqrt{5} \times 1$ superstructure[13] assuming the so-called block-checkerboard antiferromagnetic order of Fe moments.[26] In Figs. 4(a) and 4(b), the experimentally obtained spectra of $\sigma_1(\omega)$ and $\varepsilon_1(\omega)$ for the optimally-doped 122 $Ba_{0.68}K_{0.32}Fe_2As_2$ (BKFA) and 245 RFS systems are compared to the results of LDA calculations (c) and (d), respectively. Already, a direct comparison of the experimentally-obtained $\sigma_1(\omega)$ and $\varepsilon_1(\omega)$ of BKFA and RFS shows that the overall structure of the interband transitions in these two classes of superconductors is very similar apart from frequency shifts [blue and red lines in

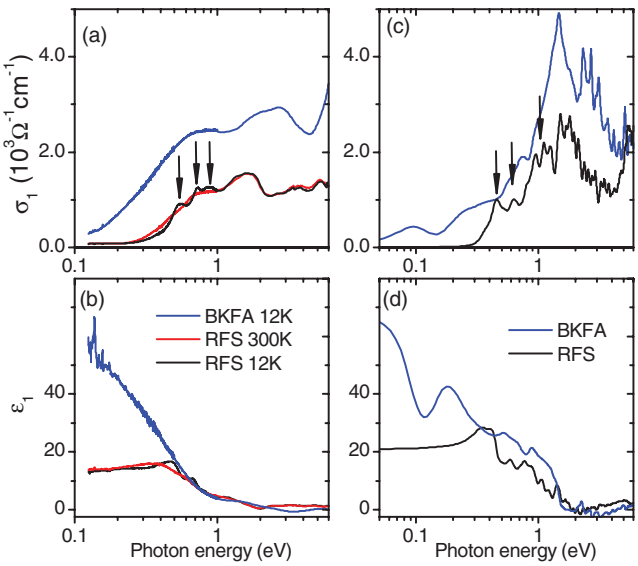

FIG. 4. (Color online) (Left panels) Comparison of the experimentally obtained real parts of the (a) optical conductivity and (b) dielectric function of an optimally doped BKFA at 12 K and RFS at 300 and 12 K. (Right panels) Same as in left panels as obtained in LDA calculations. The arrows in (a) and (c) indicate the narrow low-energy optical bands that can be resolved at low temperatures in RFS but not BKFA.

Fig. 4(a), respectively; the overall shape of the interband optical conductivity of BKFA is virtually unchanged between 300 and 10 K, see Supplemental Material in Ref. 8]. The most striking difference is the narrowing of the absorption bands in RFS around 0.6 eV at low temperatures uncovering three distinct components [black arrows in Fig. 4(a)]. Similarly, the appearance of this fine structure can be observed in the LDA calculations as shown in Fig. 4(c) for BKFA and RFS (blue and black lines, respectively, arrows indicate three possible contributions to the resolved fine structure of the 0.6-eV absorption band). In Ref. 8, it had already been shown, by subtracting the itinerant contribution to the infrared optical response of BKFA, that the low-frequency dielectric permittivity in this compound has an anomalously large value of about 60 most likely due to the high polarizability of the Fe-As bond. In RFS, the very weak and narrow free-charge-carrier response allows for determination of the low-frequency permittivity already in the raw data. Figure 4(b) compares $\varepsilon_1(\omega)$ for BKFA at 12 K (with the itinerant response subtracted[8]) and RFS at 12 and 300 K (raw data). It is clear that the low-energy permittivity of RFS is about three times smaller than that of BKFA. This trend is very well reproduced in our LDA calculations shown in Fig. 4(d), in which a comparable decrease is obtained.

Our LDA calculations show, consistent with previous work,[26,27] that the stoichiometric 245 compounds are semiconducting, and minor doping of either sign results in a very complicated Fermi surface in the magnetic state with only one type of carriers present. This is fully consistent with the weak metallic response of a nearly stoichiometric RFS observed in this Rapid Communication as well as with the overall phase diagram reported for this system in Ref. 20, where a narrow doping range was found for the superconducting phase bounded by an insulating and a semiconducting phase on the underdoped and overdoped sides, respectively. In the same Ref. 20, it was shown that the electronic specific heat exhibits a rather small superconductivity-induced anomaly at the superconducting transition temperature. Together with the small effect of superconductivity on the itinerant optical response observed here, it implies that superconductivity in RFS is not a uniform bulk phenomenon. This conclusion is also consistent with a practically doping-independent superconducting transition temperature observed in Ref. 20 assuming that the superconducting phase stabilizes at the same doping level, while the excess is doped into the coexisting phase(s).

To summarize, we obtained the complex dielectric function of an RFS superconductor with $T_c \approx 32$ K in the spectral range from 1 meV to 6.5 eV. Comparison with our LDA calculations showed that the optical response of this material can be reproduced rather well and is close to its Fe-As-based counterparts in the 122 family. Strikingly, unlike in iron pnictides, the absorption band at 0.6 eV experiences a spin-controlled narrowing into three sub-bands in the magnetic state. We further demonstrated that the superconducting RFS displays a clear metallic response in the THz spectral range below 100 K with $\omega_{pl} \approx 100$ meV, which can be divided into a narrow and a broad component and is partially suppressed in the superconducting state giving rise to a superconducting condensate with a plasma frequency of $\omega_{pl}^{SC} \approx 40$ meV. Such a small charge-carrier density suggests that the optical conductivity of the superconducting RFS represents an effective-medium response of two separate phases dominated by the magnetic semiconducting phase.

During the review process, we became aware of two closely related reports[28,29] on potassium-intercalated iron selenides. Spectral limitation and the absence of optical-phase information in reflectivity measurements led the authors to interpret the low-temperature plasma edge or small effective condensate density as the result of Josephson coupling between in-plane stripelike superconducting domains. In our measurements, full control of the signal phase down to 1 meV allowed us to conclude that the zero-crossing in the real part of the dielectric function sets in already below 100 K and is a manifestation of the inherent semiconductor-metal transition observed in all iron-selenide superconductors as a "hump" in dc resistivity peaked at approximately the same temperature.

This project was supported by the German Science Foundation under Grants No. BO 3537/1-1 and No. DE1762/1-1 within SPP 1458 as well as TRR80 (Augsburg-Munich). We gratefully acknowledge Y.-L. Mathis for support at the infrared beamline of the synchrotron facility ANKA at the Karlsruhe Institute of Technology.

[1] D. C. Johnston, Adv. Phys. **59**, 803 (2010).
[2] I. I. Mazin, Nature (London) **464**, 183 (2010).
[3] W. Z. Hu, J. Dong, G. Li, Z. Li, P. Zheng, G. F. Chen, J. L. Luo, and N. L. Wang, Phys. Rev. Lett. **101**, 257005 (2008).

[4] A. Charnukha, P. Popovich, Y. Matiks, D. L. Sun, C. T. Lin, A. N. Yaresko, B. Keimer, and A. V. Boris, Nat. Commun. **2**, 219 (2011).
[5] N. Barišić, D. Wu, M. Dressel, L. J. Li, G. H. Cao, and Z. A. Xu, Phys. Rev. B **82**, 054518 (2010).
[6] G. Li, W. Z. Hu, J. Dong, Z. Li, P. Zheng, G. F. Chen, J. L. Luo, and N. L. Wang, Phys. Rev. Lett. **101**, 107004 (2008).
[7] K. W. Kim, M. Rössle, A. Dubroka, V. K. Malik, T. Wolf, and C. Bernhard, Phys. Rev. B **81**, 214508 (2010).
[8] A. Charnukha, O. V. Dolgov, A. A. Golubov, Y. Matiks, D. L. Sun, C. T. Lin, B. Keimer, and A. V. Boris, Phys. Rev. B **84**, 174511 (2011).
[9] J. Guo, S. Jin, G. Wang, S. Wang, K. Zhu, T. Zhou, M. He, and X. Chen, Phys. Rev. B **82**, 180520 (2010).
[10] J. J. Ying, X. F. Wang, X. G. Luo, A. F. Wang, M. Zhang, Y. J. Yan, Z. J. Xiang, R. H. Liu, P. Cheng, G. J. Ye, and X. H. Chen, Phys. Rev. B **83**, 212502 (2011).
[11] Y. Mizuguchi, H. Takeya, Y. Kawasaki, T. Ozaki, S. Tsuda, T. Yamaguchi, and Y. Takano, Appl. Phys. Lett. **98**, 042511 (2011).
[12] A. F. Wang, J. J. Ying, Y. J. Yan, R. H. Liu, X. G. Luo, Z. Y. Li, X. F. Wang, M. Zhang, G. J. Ye, P. Cheng, Z. J. Xiang, and X. H. Chen, Phys. Rev. B **83**, 060512 (2011).
[13] J. Bacsa, A. Y. Ganin, Y. Takabayashi, K. E. Christensen, K. Prassides, M. J. Rosseinsky, and J. B. Claridge, Chem. Sci. **2**, 1054 (2011).
[14] W. Bao, Q. Huang, G. F. Chen, M. A. Green, D. M. Wang, J. B. He, X. Q. Wang, and Y. Qiu, Chin. Phys. Lett. **28**, 086104 (2011).
[15] J. T. Park, G. Friemel, Y. Li, J.-H. Kim, V. Tsurkan, J. Deisenhofer, H.-A. Krug von Nidda, A. Loidl, A. Ivanov, B. Keimer, and D. S. Inosov, Phys. Rev. Lett. **107**, 177005 (2011).
[16] A. Ricci *et al.*, Phys. Rev. B **84**, 060511 (2011).
[17] W. Li, H. Ding, P. Deng, K. Chang, C. Song, K. He, L. Wang, X. Ma, J.-P. Hu, X. Chen, and Q.-K. Xue, Nat. Phys. **8**, 126 (2012).
[18] M. Wang *et al.*, Phys. Rev. B **84**, 094504 (2011).
[19] Z. G. Chen, R. H. Yuan, T. Dong, G. Xu, Y. G. Shi, P. Zheng, J. L. Luo, J. G. Guo, X. L. Chen, and N. L. Wang, Phys. Rev. B **83**, 220507 (2011).
[20] V. Tsurkan, J. Deisenhofer, A. Günther, H.-A. Krug von Nidda, S. Widmann, and A. Loidl, Phys. Rev. B **84**, 144520 (2011).
[21] V. Ksenofontov, G. Wortmann, S. A. Medvedev, V. Tsurkan, J. Deisenhofer, A. Loidl, and C. Felser, Phys. Rev. B **84**, 180508 (2011).
[22] A. V. Boris, N. N. Kovaleva, S. S. A. Seo, J. S. Kim, P. Popovich, Y. Matiks, R. K. Kremer, and B. Keimer, Phys. Rev. Lett. **102**, 027001 (2009).
[23] F. Ye, S. Chi, W. Bao, X. F. Wang, J. J. Ying, X. H. Chen, H. D. Wang, C. H. Dong, and M. Fang, Phys. Rev. Lett. **107**, 137003 (2011).
[24] A. I. Coldea, C. M. J. Andrew, J. G. Analytis, R. D. McDonald, A. F. Bangura, J.-H. Chu, I. R. Fisher, and A. Carrington, Phys. Rev. Lett. **103**, 026404 (2009).
[25] H. Shishido *et al.*, Phys. Rev. Lett. **104**, 057008 (2010).
[26] X.-W. Yan, M. Gao, Z.-Y. Lu, and T. Xiang, Phys. Rev. B **83**, 233205 (2011).
[27] C. Cao and J. Dai, Phys. Rev. Lett. **107**, 056401 (2011).
[28] R. H. Yuan, T. Dong, Y. J. Song, P. Zheng, G. F. Chen, J. P. Hu, J. Q. Li, and N. L. Wang, Sci. Rep. **2**, 221 (2012).
[29] C. C. Homes, Z. J. Xu, J. S. Wen, and G. D. Gu, e-print arXiv:1110.5529.